

**Filtering. Thermal noise - attenuation chain**

**DC-blocks**

**Coaxials, circulators**

#### **5.1.2. Thermal noise**

#### **5.1.3. Shielding**

**Magnetic shielding**

**IR shielding**

#### **5.1.4. Amplification chain. JPA, TWPA, HEMT – active elements at cold temperature**

#### **5.1.5. DC-lines**

Its necessary to have the dc lines inside the cryogenic setup for many reasons. first we need a power supply to feed the HEMT amplifiers, based on 4K plate, and second we need a dc current to provide a magnetic field to bias the squids of qubit and JPA/TWPA amplifiers. also this lines can be used to make a gate voltage for some types of qubits, or, bias the microwave switch for example.

#### **5.1.6. Dilution refrigerators (Big fridge, Bluefors, work principles, pulse-tube)**

### **5.2. Microwave at room-temperature setup**

Time domain scheme, VNA, current sources, acquisition board

- 5.2.1. VNA measurements of transmission**
- 5.2.2. Homodyne-heterodyne measurements**
- 5.2.3. Signal forming (SSB, Mixers, AWG)**
- 5.3. Digital part: signal forming, acquisition, data analysis, qtlab**
  - 5.3.1. Signal forming for AWG**
  - 5.3.2. Acquisition (demodulation, IQ-mixer, filtering amplification)**
  - 5.3.3. Device synchronisation and triggering**
  - 5.3.4. Data analysis**
  - 5.3.5. Python, qtlab**
  - 5.3.6. My contributions to the code of measurements and analysis**

## **5.4. Chapter key points**

In this chapter we described all parts of our measurement setup. The low-temperature components as well as the cryogenic setup were presented. The principles of qubit packaging were briefly defined. The principles of protecting the qubit from external influences: such as high-frequency noise, magnetic field, and infrared illumination were presented. The principles of microwave pulse generation were discussed as well.



# Chapter 6.

## Measurements – Results

The determination of this chapter is devoted to microwave measurements of three samples with transmon molecules. It is divided into subsections according to the type of measurements taken.

(i) First, we will discuss microwave spectroscopy conducting single-tone and two-tone measurements. We will determine the working frequencies of the qubit and polaritons for further work. Using the frequencies we will extract the exact electrical parameters of our system to compare them with those of earlier generations of transmon molecules. The acquired data will be used as important feedback to improve the fabrication process and design of new qubits.

(ii) The second section on time-domain microwave measurement is devoted to the study of qubit coherence. The main focus will be on measuring times  $T_1$ ,  $T_2$  and  $T_{Rabi}$  under different conditions. With these studies we aim to estimate how coherence times have been changed as a result of the design modifications and a new fabrication recipe. A detailed presentation of the improvements which were implemented is provided in other chapters.

(iii) Finally, in the third section, we will continue time-domain measurements with the goal of reading the state of the qubit. It presents the results of a single-shot qubit readout. We will also discuss high fidelity and quantum nondemolition of the readout as well as quantum trajectories. This data will be used for comparison with the state-of-the-art solutions in the field of cQED systems. It will allow us to estimate the prospects of transmon molecules with cross-Kerr coupling for quantum computation.

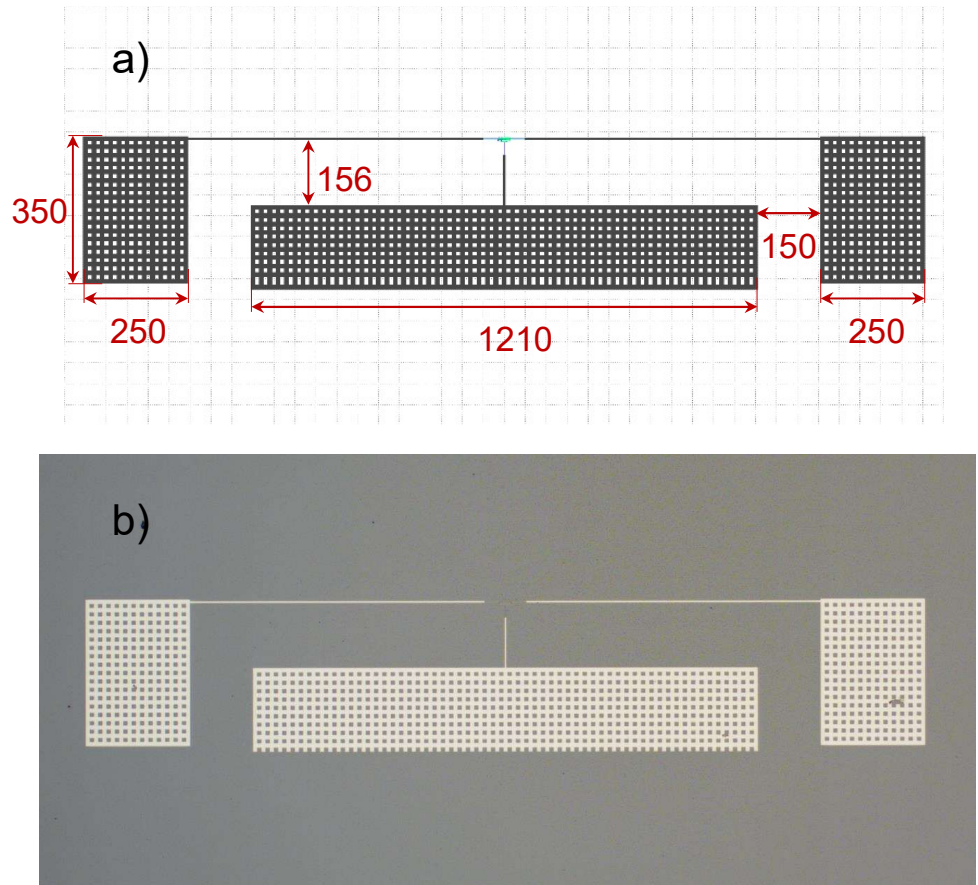


Figure 6.1. a) - Design of *Sample-A*, projected by Remy Dassonneville. All sizes are given in  $\mu m$ . Width of wires is  $4\mu m$ . Size of holes is  $10 \times 10\mu m$ . b) - Optical microscopy of *Sample-A* after measurements.

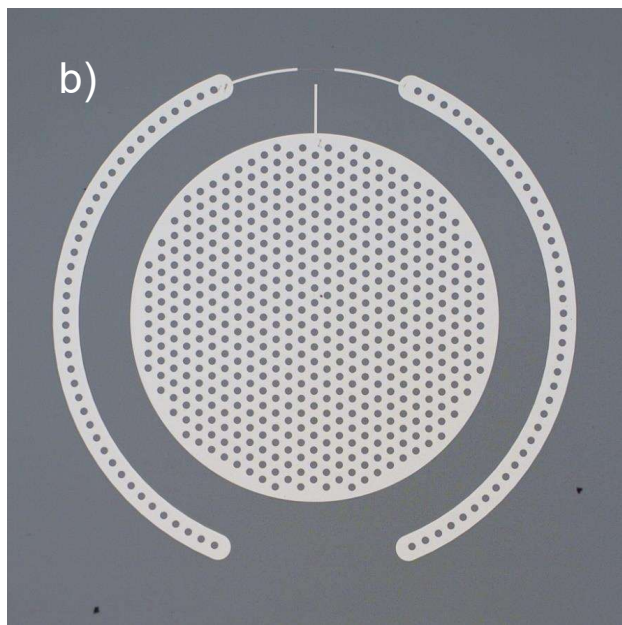
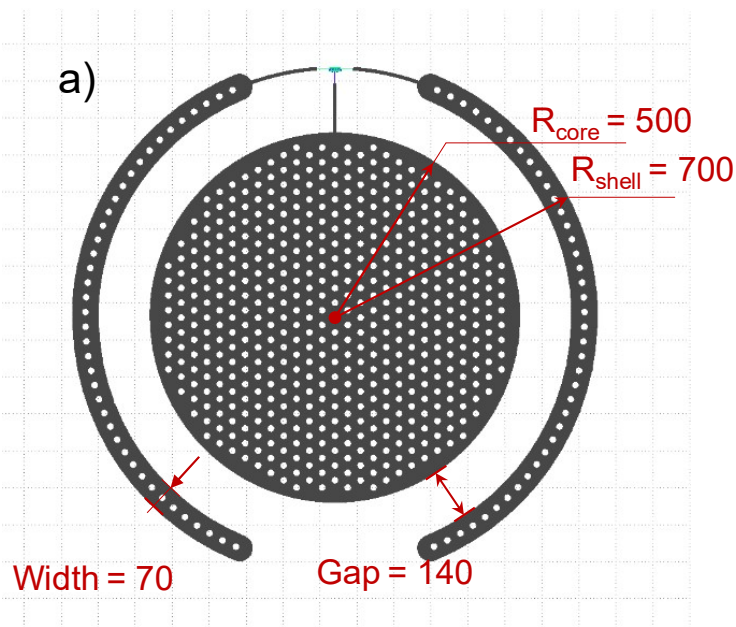


Figure 6.2. a) - Design of *Sample-B*, projected by me during my PhD. All sizes are given in  $\mu\text{m}$ . Width of wires is  $8\mu\text{m}$ . Diameter of holes is  $20\mu\text{m}$ . b) - Optical microscopy of *Sample-B*.

## 6.1. Introducing three samples ("A","B","C")

In this chapter, the reader will be presented with the main results of microwave measurements of three different samples. The first sample, *Sample-A* was fabricated by Remy Dassonneville during his PhD project and has already been described in the following works [69], [71]. This sample was characterized by high fidelity levels. However, several problems were detected. This system had a low relaxation time ( $3.3 \mu s$ ) which limited the fidelity of readout. In addition, high non-linearity of ancilla mode prevented the increase of readout speed by increasing the readout power. To face these challenges the second and third samples (*Sample-B*, *Sample-C*) were created by the author of the manuscript and are described for the first time. In *Sample-B* a new circular design was applied, described in detail in Chapter 3 - "Engineering of transmon molecule". The design changes were implemented based on the studies of *Sample-A* with an intention to improve the coherence times of the qubit. In this case, a standard fabrication recipe developed for *Sample-A* was used to make an isolated comparison for the design factor. However, with the *Sample-C* an improved fabrication recipe was applied to complement the design benefits.

*Sample-A* is the first generation of 3D transmon molecules. At this time the purpose of *Sample-A* was to implement transmon molecules in 3D architecture and to demonstrate the novel readout through polariton.

*Sample-B* was the second transmon molecule generation. Its main goals were: (i) to minimize the residual transverse coupling by using the circular shape of the pads reducing the dipole momentum of the qubit; (ii) to explore new readout possibilities in the case of a less nonlinear ancilla; (iii) to increase the detuning between the qubit and the polariton readout frequency. As previously stated, the new design described in Chapter 3 was used to produce this sample.

*Sample-C* was based on the same design as *Sample-B*. The goal of this third-generation was to extend the coherence times of the transmon molecule based on the optimized fabrication recipe described in Chapter 4.

## 6.2. Spectroscopy of polaritons and qubit

In this section we will present measurements using continuous microwave spectroscopy. These measurements are made at the beginning in order to

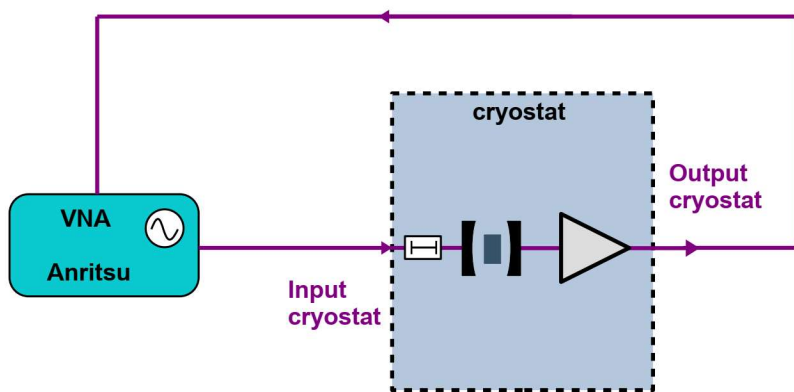


Figure 6.3. Schematic of a simple single-tone spectroscopy measurement. The VNA output is connected to the input port of the fridge. The VNA input is connected through a room temperature amplifier "ZVA-183-S+" to the fridge output.

determine the frequencies of the qubit and the readout mode.

### 6.2.1. Single-tone spectroscopy

In order to implement single-tone spectroscopy we connect a vector network analyzer (**VNA**) to the setup as it is shown in the Fig. 6.3. We measure the transmission of a continuous microwave signal propagating through a 3D cavity interacting with the chip inside. Technically, VNA compares the signal passing through the setup with a reference signal. It measures the transmission coefficient in amplitude and phase. The signal sent by the VNA is called the probe signal. By varying the frequency of the probe signal, we can observe a peak in amplitude in transmission and a strong phase variation that corresponds to the resonant frequency of the 3D-cavity.

#### Bare 3D-cavity at 4K

At temperatures above the critical superconductivity temperature for aluminum, we can measure the bare 3D-cavity frequency. Of course, in fact, the copper cavity's own resonant mode interacts with the silicon chip inside. However, at 4K the interaction with the aluminum microstructure can be neglected since the circuit remains highly resistive. The result of single-tone spectroscopy at around 4K is shown on Fig. 6.4. The frequency of the peak is around  $7.253\text{GHz}$  and corresponds to the  $TE_{101}$  mode of this cavity.

Then, when the temperature decreases below the critical temperature, the phase transition of aluminum to superconductivity occurs. The modes of the qubit and ancilla associated with the aluminum device emerge. Because of the strong coupling, the ancilla and cavity form two polaritons. So we can see a shift in the resonant frequency on our single-tone spectroscopy during cooling.

See Fig. 6.4 b) and d).

#### Polariton spectroscopy vs magnetic flux

Once the system has cooled down to a very low temperature ( $T \approx 30\text{mK}$ ), we observe two polaritons - hybridization of the 3D-cavity and ancilla modes.

Fig. 6.6 presents the result of single-tone spectroscopy as function of the external magnetic field. Fig. 6.6 a), b) show measured amplitude of transmitted signal. Each of the plots has the probe frequency on Y axis,

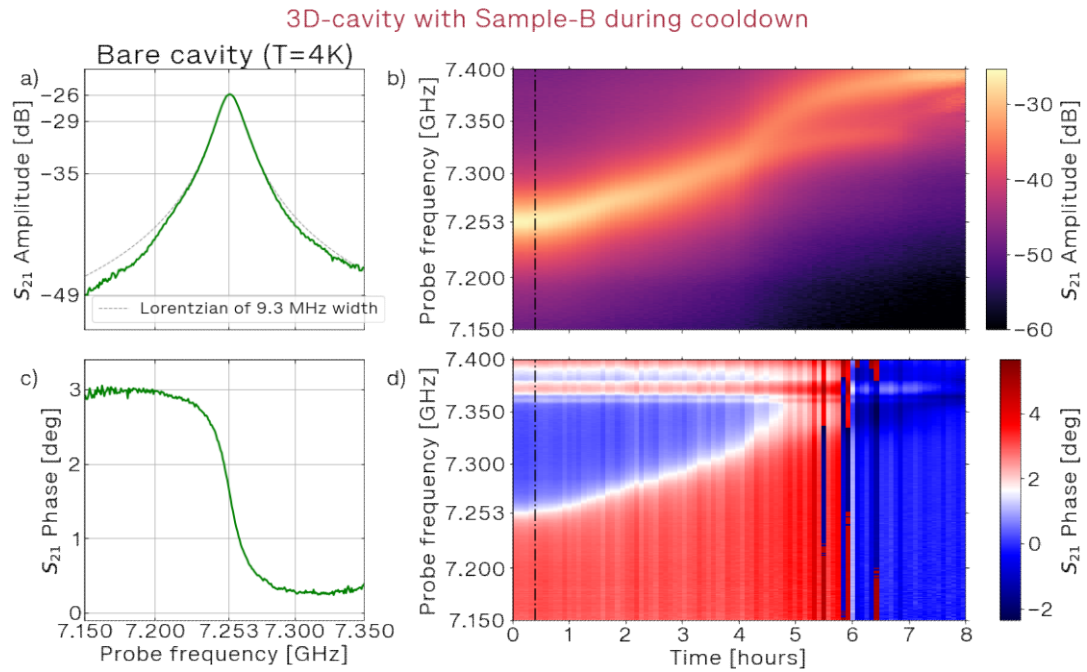


Figure 6.4. a), c) - Single-tone spectroscopy of the bare 3D-cavity measured at  $4K$ .  $S_{21}$  amplitude and  $S_{21}$  phase respectively are shown as a function of probe frequency. The green line shows measurement data, and the dashed grey line depicts the fit of Lorenzian function. Its frequency is 7.253 GHz and the full width at half maximum equals to 9.3 MHz. b), d) - Single-tone spectroscopy as a function of time recorded as the temperature decreased from  $4K$  to  $50mK$ . The amplitude (orange to purple) and the phase change (red to blue) are depicted versus frequency of probe and time. We observe that the transmission peak moves from  $7.25GHz$  to about  $7.4GHz$ .

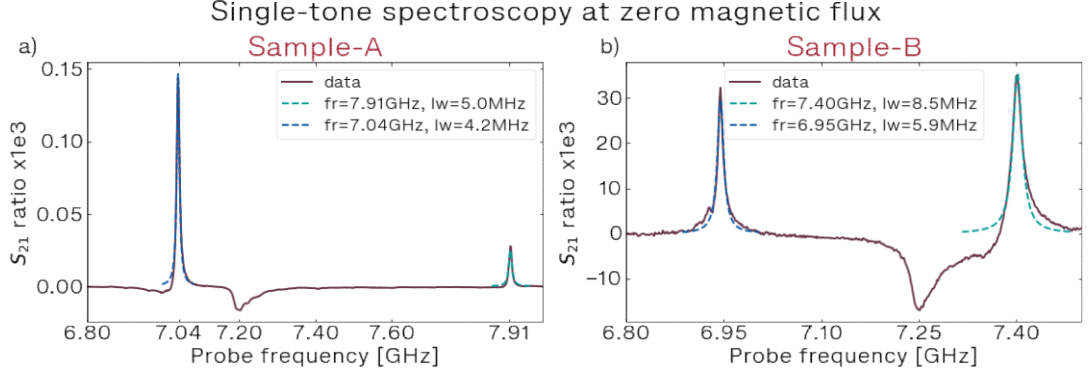


Figure 6.5. Single-tone spectroscopy of two polaritons a) - *Sample-A* and b) - *Sample-B*. Both plots depict the transmission of signal amplitude as a linear ratio vs frequency at zero magnetic flux. We observe the two peaks which fit the Lorenzian curves at frequencies of  $7.04\text{GHz} \pm 1\text{MHz}$  and  $7.91\text{GHz} \pm 1\text{MHz}$  for *Sample-A* and  $6.95\text{GHz} \pm 1\text{MHz}$  and  $7.40\text{GHz} \pm 1\text{MHz}$  for *Sample-B*.

the number of magnetic flux quanta  $\frac{\Phi}{\Phi_0}$  on the bottom axis, and the supply current corresponding to this flux on the upper axis. The two resonant peaks of polariton are observed as two maxima of amplitude. These peaks show a strong dependence on the external magnetic field. We observe a rapid periodic oscillations of both polariton's frequencies. We observe a smooth change in the frequencies of both polaritons, modulated by rapid periodic oscillations. Since the transmon molecule contains superconducting loops, we can change its characteristics by applying an external magnetic field, thus influencing the polariton frequency. The larger one, associated with the qubit, causes fast oscillations of the polariton. Whereas small loops of SQUIDS, constituting the inductor is responsible for the slow change of polariton frequency. We observe a little difference between zero of current (on top axis) and zero of magnetic flux (bottom axis). This can be explained by presence of environmental magnetic field during cooling of the setup, penetrated through the magnetic shield. (Notice that magnetic field of the Earth is around  $25\text{-}65\ \mu\text{T}$ ) [72], [73].

It is in the local maxima of polaritons that the so-called sweet-spots are located. In these points the system is less sensitive to magnetic noise. It is preferable to measure there to maximize the relaxation time of the qubit. In our case, it is especially important to measure in the sweet-spots, since only there the symmetry conditions necessary for the existence of cross-Kerr

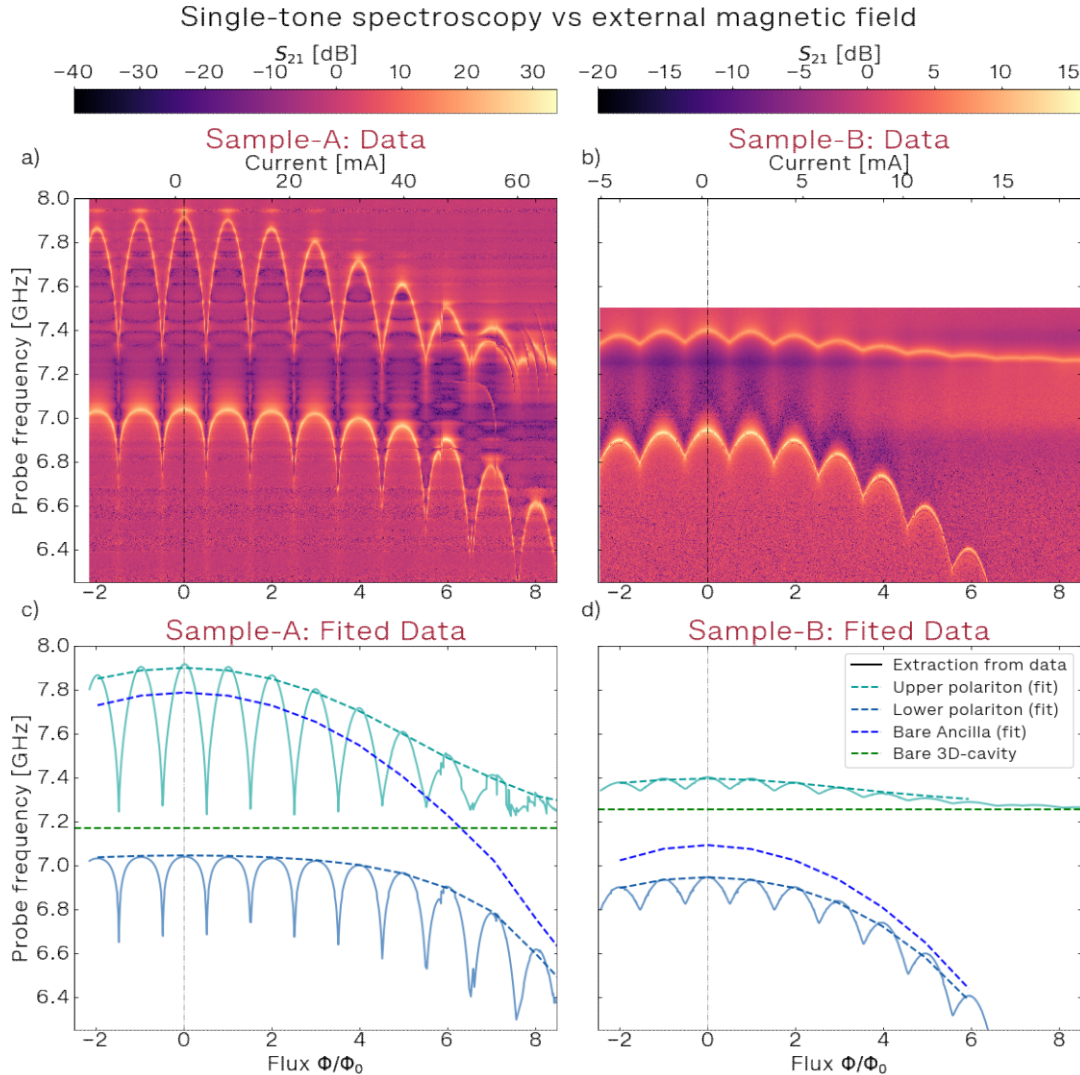


Figure 6.6. Single-tone spectroscopy vs external magnetic field. To generate the magnetic field, we apply a current through a coil of superconducting wire located near the cavity. On the Y axis is the frequency of the VNA, on the X-axis is the integer number of flux going through a loop, correspond to qubit and the current needed for this.

coupling are fulfilled.

On Fig. 6.6 c), d) it is shown fits of this data. Solid lines corresponds to values of amplitude peaks extracted from the data. Green horizontal line shows the frequency of bare cavity, measured before. Blue line in an extracted frequency of bare ancilla. Sea-color and steel-color dashed lines corresponds to extracted polaritons frequencies.

To fit these curves we used the protocol described in detail in [71]. From the single-tone we obtain frequencies of two polaritons and bare cavity:  $\bar{\omega}_l$ ,  $\bar{\omega}_u$  and  $\omega_c$ . Than from two-tone spectroscopy 6.2.2 we obtain qubit frequency:  $\omega'_q$ . From this values we calculate the frequency of ancilla when qubit is in ground state:  $\bar{\omega}_a = \bar{\omega}_l + \bar{\omega}_u - \omega_c$ , and a bare ancilla frequency:  $\omega'_a = \bar{\omega}_a - g_{zz}$ , where ancilla-qubit cross-Kerr coupling  $g_{zz}$  is fitted from flux dependence. Using formula:

$$\omega_{u,l}^2 = \frac{\omega_a^2 + \omega_c^2}{2} \pm \frac{1}{2} \sqrt{(4g_a)^2 \omega_a \omega_c + (\omega_a^2 - \omega_c^2)^2} \quad (6.1)$$

we extracted ancilla-cavity coupling  $g_{ac}^A/2\pi=295$  MHz for *Sample-A* and  $g_{ac}^B/2\pi=209$  MHz for *Sample-B* from the polaritons anti-level crossing, knowing  $\omega_a$ . The model used to derive this equation is considered that ancilla and cavity modes interact strongly, which is true in our case.

The next step is to extract the mixing angle  $\theta$ , given by  $\theta = \frac{1}{2} \arctan \left( \frac{2g_{ac}}{\omega_a - \omega_c} \right)$  which reflects the proportion of ancilla and cavity in each polariton. The extracted  $\theta$  as a function of magnetic flux quanta is presented on Fig. 6.7.

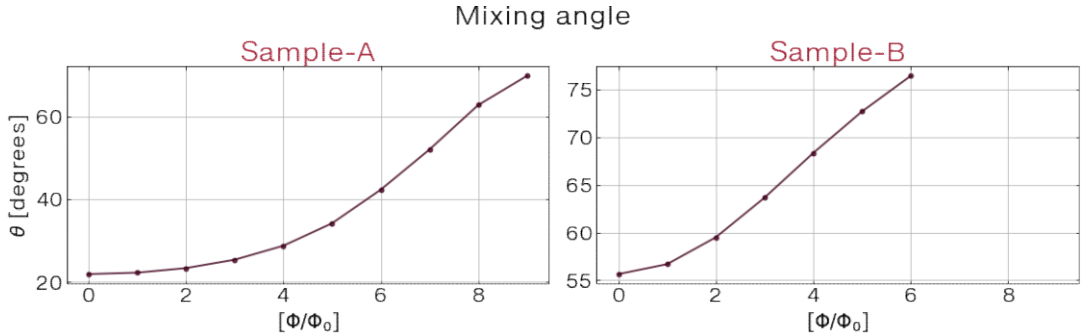


Figure 6.7. Mixing angle between ancilla and cavity corresponded to each flux number. The range of values of this parameter lies within  $0^\circ$  to  $90^\circ$ . The more this angle is close to  $90^\circ$  the more lower polariton is ancilla-like, and upper polariton is cavity-like. And otherwise: the more  $\theta$  is close to  $0^\circ$  the more lower polariton is cavity-like, and upper polariton is ancilla-like.

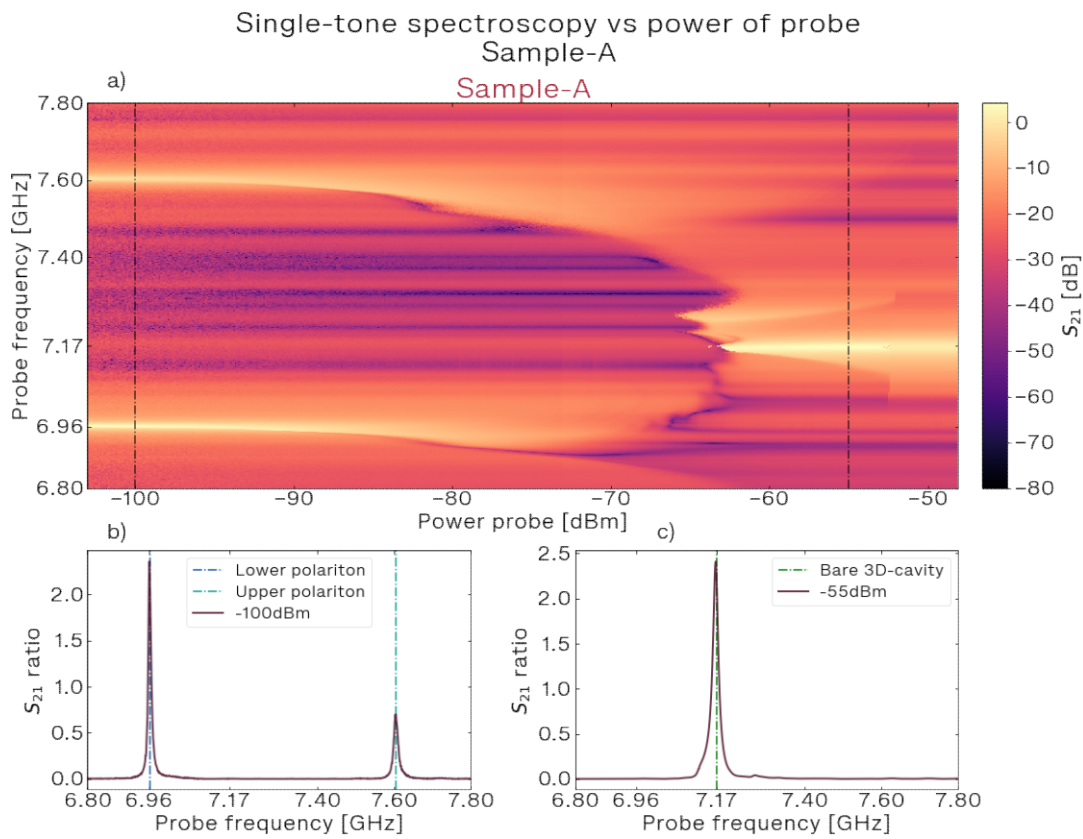


Figure 6.8. a) - Single-tone spectroscopy as a function of probe power and frequency for *Sample-A*. On the X-axis the power of the probe estimated at the entrance of the 3D-cavity. The Y axis is the frequency of the probing signal sent by the VNA. The color bar reflects the amplitude of the probe signal transmission. b), c) - Single-tone spectroscopy at given powers of probe (-100 dBm and -55 dBm respectively).

## Single-tone polariton spectroscopy vs power. Polariton Lamb shift

We study the modification of the mode of the polariton when the power of the probe signal increases. We need this measurement to rationally select the power of the probe signal. For this purpose, we choose the sweet spot of a low magnetic field with the integer number of flux equal to zero and conduct single-tone spectroscopy by increasing the probe power. The result of this measurement can be seen on Fig. 6.8 a). The graph shows the amplitude of transmitted signal as a function of frequency and probe power.

At low power (Fig.6.8 b) ), we observe two resonant peaks, well-fit by the Lorentz function at about  $7GHz$  and  $7.6GHz$ . As the probe power increases, the maximum transmission shifts toward lower frequencies. At high power around  $-55dBm$  (Fig.6.8 c), the two transmission peaks disappear and are replaced by single Lorentzian peak at frequency of  $7.17GHz$ , which is similar to a bare cavity frequency.

These observations can be explained as follows: at low power, we have cavity dressed by coupling with the transmon molecule circuit. Its frequency is shifted by the Lamb shift. When the power is increased, the non-linearity of the ancilla starts causing influence resulting in the frequency shift.

If the signal power at the resonator input exceeds a value of about  $-60dBm$  we again observe a single peak corresponding to the bare 3D-cavity frequency. This is because once the critical signal strength is reached, our superconducting circuit loses superconductivity.

For further measurements we will use a probe signal power that does not cause significant frequency shift.

### 6.2.2. Two-tone spectroscopy

Our next goal is to perform measurements of the qubit mode of the transmon molecule. Since the qubit frequency lies far from the cavity frequency, we do not see it directly, because cavity acts as a filter. To measure qubit frequency, it is necessary to perform two-tone spectroscopy. For this measurement we add a second microwave source in addition to the initial VNA setup like it is shown on Fig. 6.9. The signal produced by this source is called pump signal.

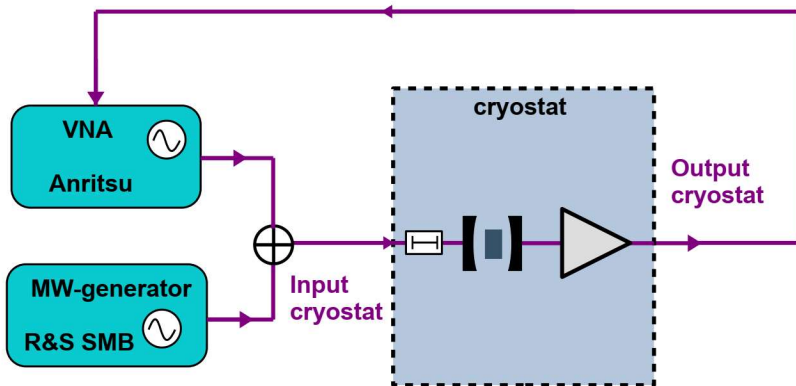


Figure 6.9. Schematic of a two-tone spectroscopy measurement. We use a microwave splitter to add the probe signal from the VNA and the pump signal from the microwave generator. Both signals are fed to the first pore of the resonator. Then the output signal is amplified and fed to the VNA input.

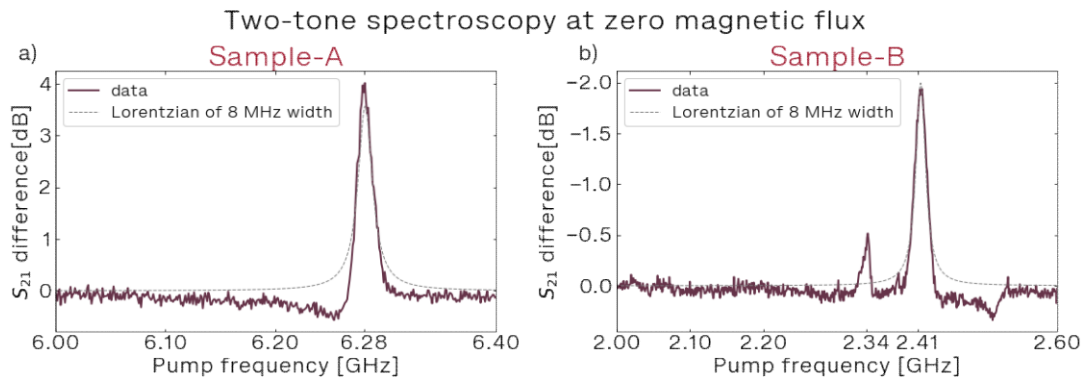


Figure 6.10. Result of two-tone spectroscopy experiment. On the X-axis the frequency of the pump. The frequency probe was fixed in the vicinity of the resonance frequency of the polariton. On the Y axis is the amplitude of the probe frequency pass-through. It can be seen that when pump frequency reaches a certain value, the amplitude of probe frequency transmission changed.

## Qubit frequency

We notice the frequency shift of the resonator when the qubit changes its state. This shift occurs due to our cross-Kerr coupling [71]. To perform two-tone spectroscopy we scan the frequency of the pump signal while continuing to measure the transmission of the probe signal through the cavity. The probe signal frequency is usually selected close to the polariton resonance. When the pump frequency coincides with the qubit's frequency, the qubit is partially excited. This causes a shift in the polariton frequency. Consequently, a change in the transmission at the probe frequency is observed.

As a result we have determined the transition frequency  $|0\rangle \rightarrow |1\rangle$  of the qubit.

The result of this measurement is shown in Fig. 6.10. On the X-axis the pump frequency is now plotted, while the probe frequency has been fixed. We observe a change in the transmission of the probe signal when the pumping signal frequency corresponds to the qubit frequency. The change in transmission is due to a shift in polariton frequency. A more detailed experiment demonstrating the effect of polariton frequency shift is described here: 6.3.3.

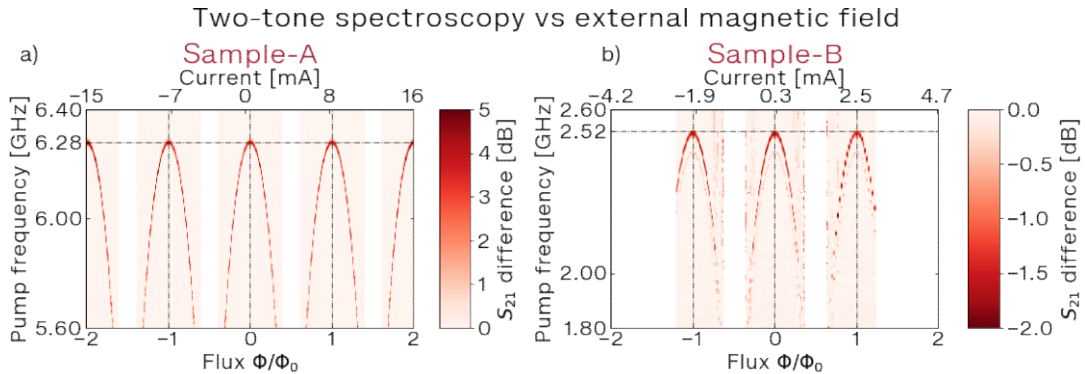


Figure 6.11. Two-tone spectroscopy vs external magnetic flux made for *Sample-A* a) and *Sample-B* b). Bottom axes shows an integer number of magnetic flux quanta, and top axes shows the current in coil, correspond to this flux. Left axes shows pump frequency. The color corresponds to transmission amplitude of probe signal. For each flux we observe a change of probe transmission at some pump frequency.

## Qubit frequency vs magnetic flux

In Fig. 6.11 we plot the transmitted probe signal as function of the frequency pump and the magnetic flux. We observe the change of qubit frequency from the magnetic field. Its maximum is around  $6.28\text{GHz}$  for *Sample-A* and  $2.52\text{GHz}$  for *Sample-B*. Qubit frequency behaves periodically and its maximums are almost the same. We have already seen the same periodicity by observing the change of polariton frequency from the magnetic field. This period corresponds to a magnetic flux quantum  $1\Phi_0$  through the big loop of the transmon molecule. For *sample-A* area of this loop is about  $S_{Loop_Q} = 5\mu\text{m} \times 28\mu\text{m}$ . Since one quantum of magnetic flux corresponds to a coil current of about  $870\mu\text{A}$ , we can estimate the magnetic field in the sample as about  $2\mu\text{T}$ . Thus, we establish dependence between quantized magnetic flux passing through the circuit loop and the electric current in the magnetic coil. Since the frequency of the qubit is sensitive on the magnetic field than the polariton frequency, we accurately determine the current value for the sweet spot.

## Qubit frequency vs power of pump

To extract the anharmonicity of the qubit mode we probe the higher-order transitions. For this purpose, we increase the pump signal power until we find other peaks. As a rule, a peak corresponding to transition frequency  $|1\rangle \rightarrow |2\rangle$  appears first. This transition occurs when the qubit is already in state  $|1\rangle$ , for example, due to thermal excitation. When the pumping power is high enough, the peak associated to the two-photon transition  $|0\rangle \rightarrow |2\rangle$  can be also detected. The result of this experiment is depicted in Fig. 6.12. This two-photon transition  $\frac{\omega_{2,1}}{2}$  is located between the qubit transition  $\omega_{0,1}$  and  $\omega_{1,2}$ . The anharmonicity of the qubit is extracted through the formula:  $\alpha_Q = \omega_{2,0} - 2\omega_{1,0}$

## AC-Stark effect. Qubit frequency vs power of probe tone

Qubit AC-Stark shift is a frequency shift of the qubit induced by the occupation of the resonator mode by photons. In our case, the role of the resonator will be played by a polariton. We perform the two-tone spectroscopy measurements by increasing probing signal power. Fig. 6.13 illustrates the result of this experiment. When selecting the readout power, we will be guided by this graph, trying to stay in a mode where this shift does not occur.

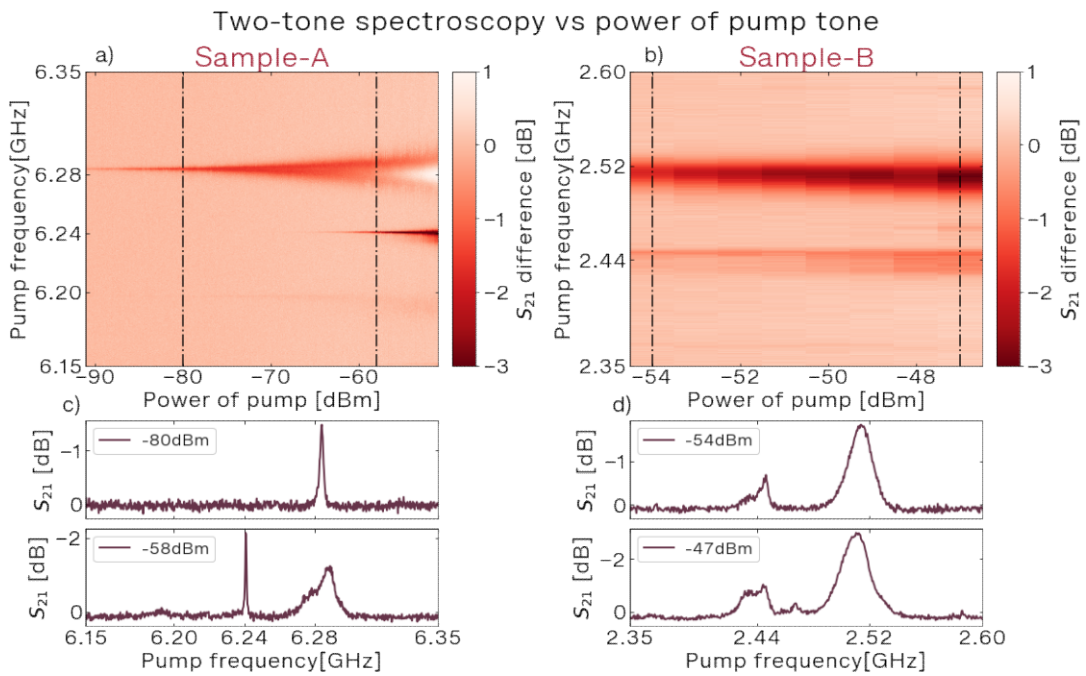


Figure 6.12. a), b) - Two-tone spectroscopy as a function of power and frequency of pump tone. As the power increases, there are more transitions between the energy levels of the qubit. Due to this it is possible to extract values of qubit anharmonicity  $\alpha_Q$ . c), d) - Two-tone spectroscopy at a given pump powers. The frequencies of the peaks are  $6.24\text{GHz}$  and  $6.28\text{GHz}$  for *Sample-A* and  $2.44\text{GHz}$  and  $2.52\text{GHz}$  for *Sample-B*.

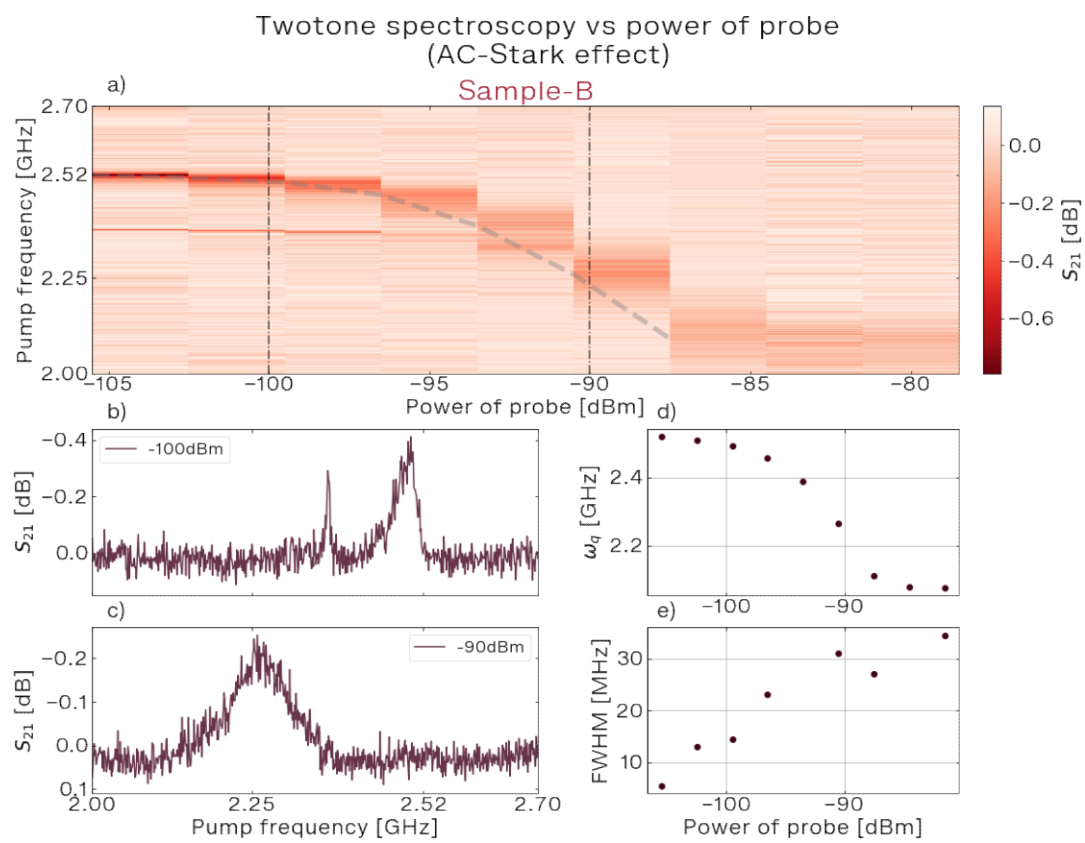


Figure 6.13. Two-tone spectroscopy vs variation of power of probe tone for *Sample-B*.

### 6.2.3. Conclusions of spectroscopy measurements

After performing spectroscopic studies, we can draw conclusions about the characteristics of the resulting *sample-B* and compare them with the target characteristics as well as with the characteristics of *sample-A*.

Spectroscopic and electrical characteristics comparison			
Characteristics	<i>Sample-A</i>	<i>Sample-B</i> (target)	<i>Sample-B</i>
$Freq_Q$ [GHz]	6.284	2.78	2.523
$Freq_A$ [GHz]	7.78	7.35	7.092
$\alpha_Q$ [MHz]	-88	-77	-76.2
$U_A$ [MHz]	-13.5	-1.3	-1.92
$g_{zz}$ [GHz]	34.5	10.1	13.6
$C_s$ [ $fF$ ]	110	125	129
$C_t$ [ $fF$ ]	59.6	123	83.5
$E_j$ [GHz/ $2\pi\hbar$ ]	29.2	7.3	5.76
$L_A$ [ $nH$ ]	5.32	2.66	3.59

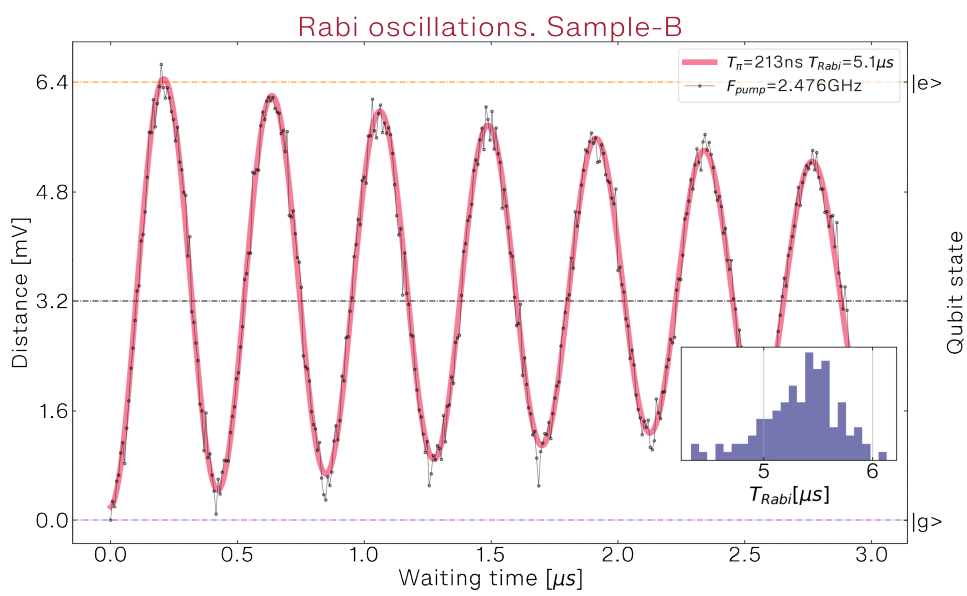


Figure 6.14. Rabi example

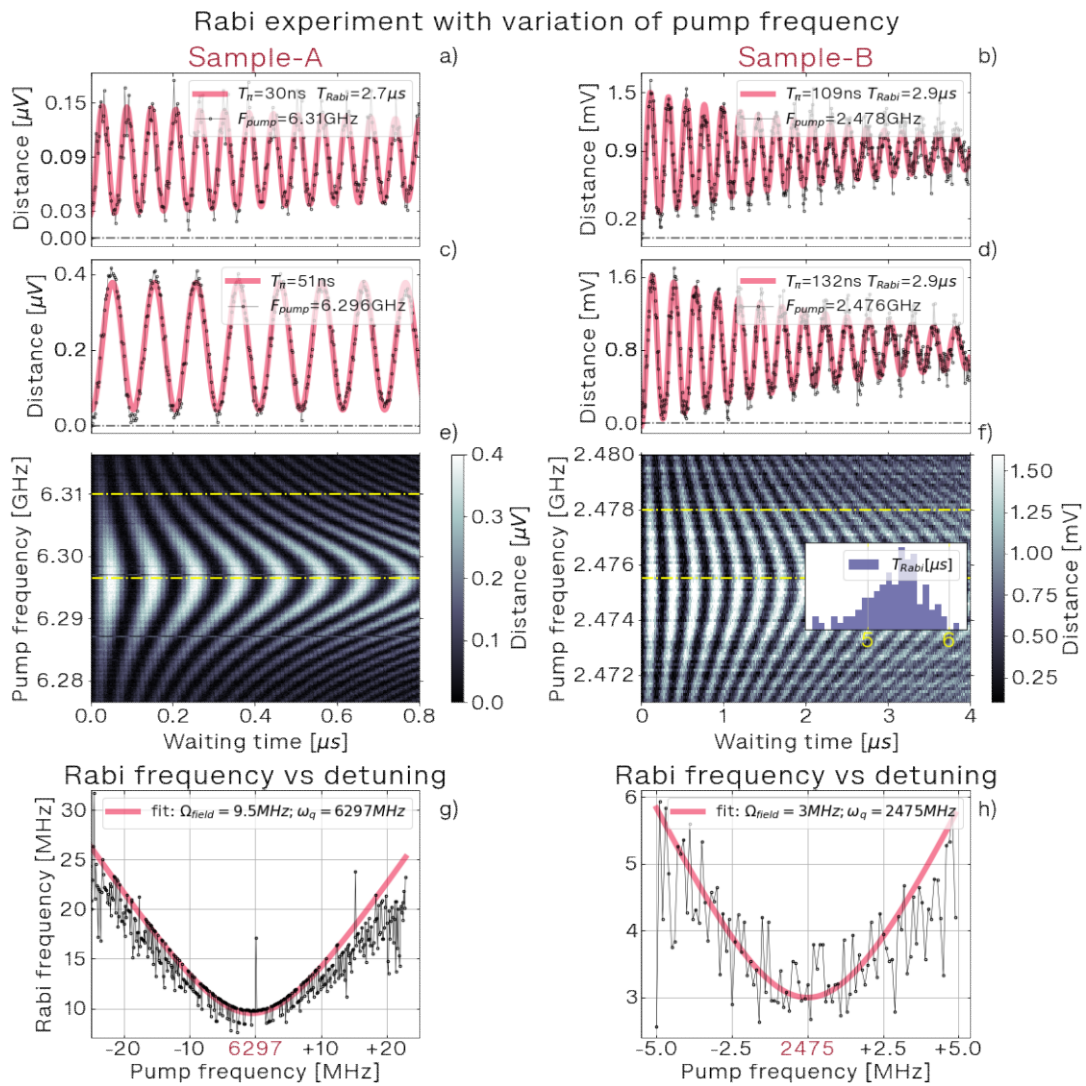


Figure 6.15. Rabi chevrons

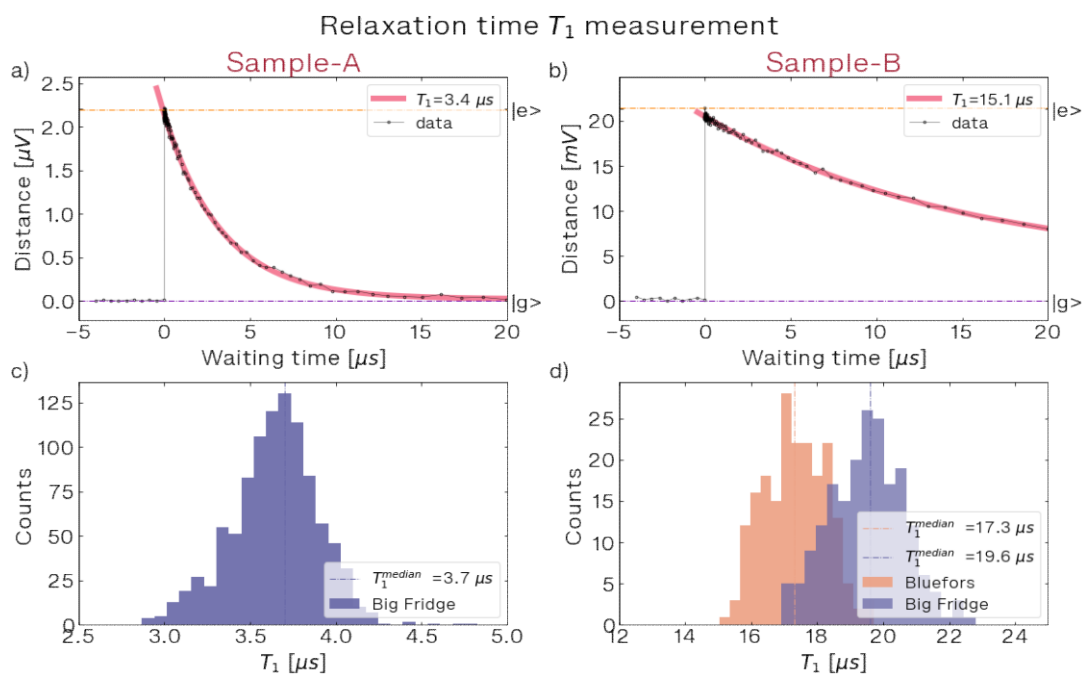


Figure 6.16.  $T_1$  Relaxation A and B

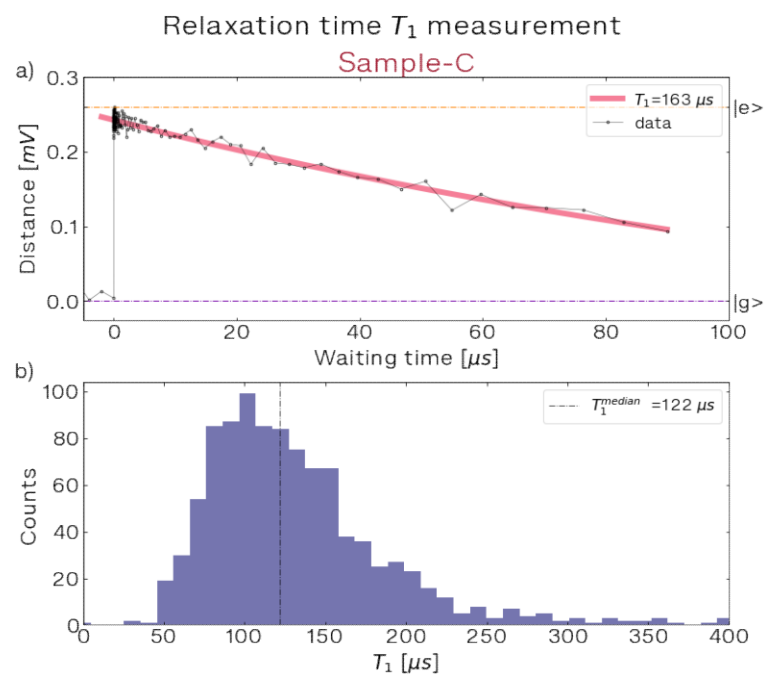


Figure 6.17.  $T_1$  Relaxation C

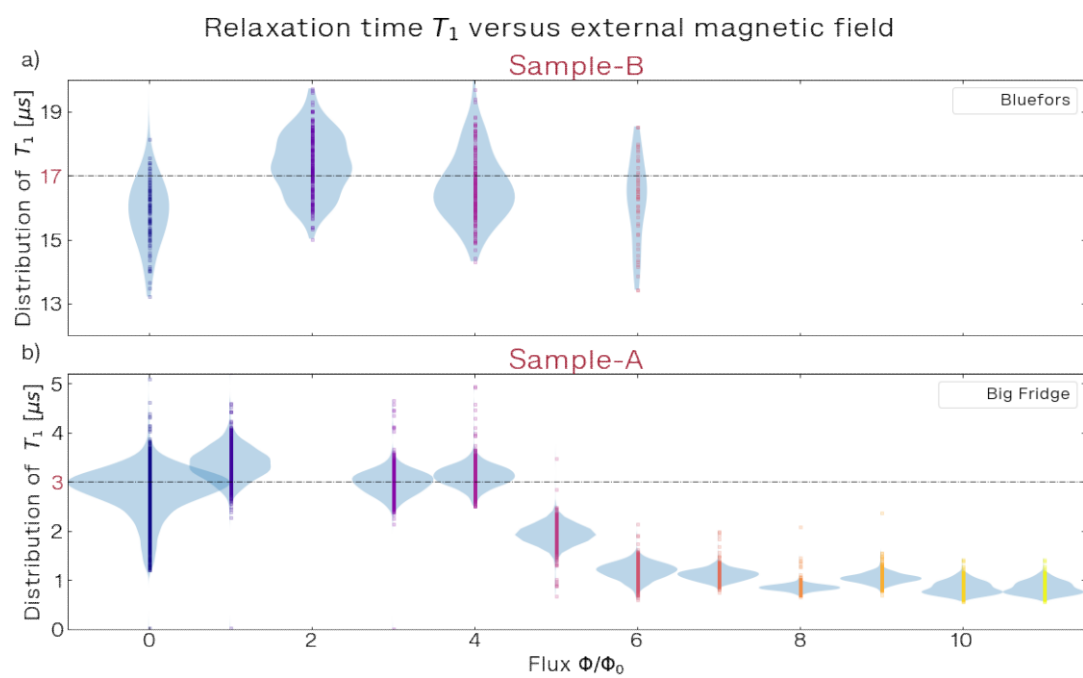


Figure 6.18.  $T_1$  vs flux

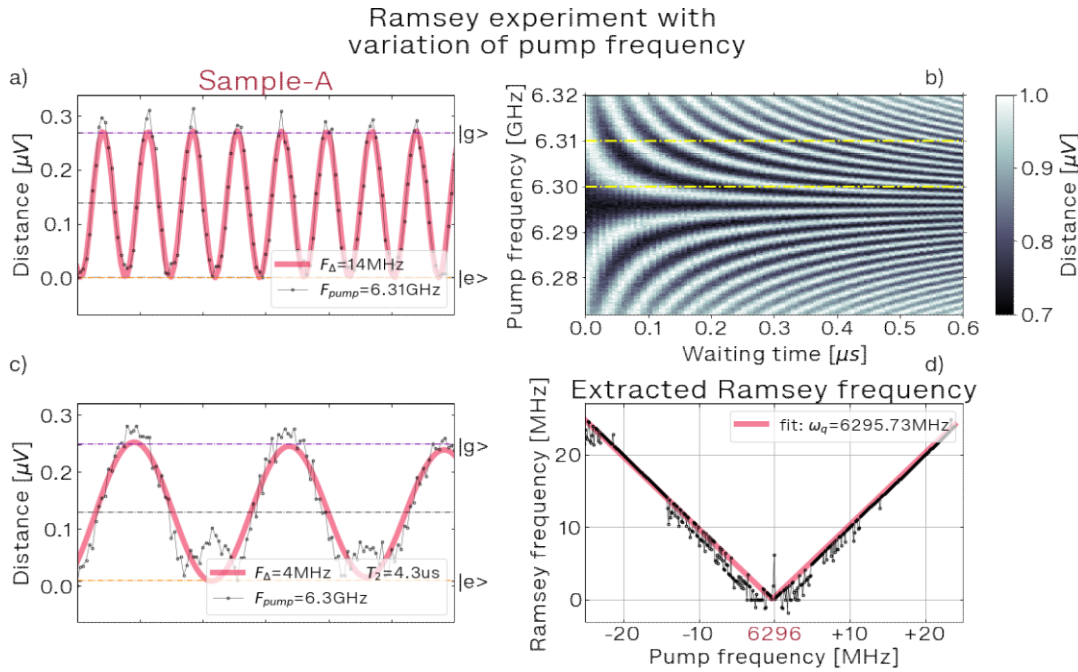


Figure 6.19. Ramsey fringes

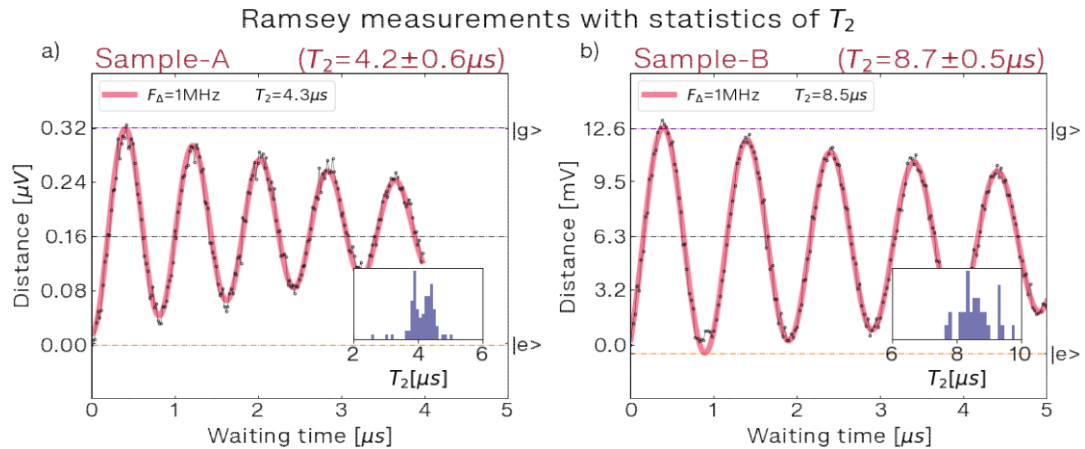


Figure 6.20.  $T_2$  statistics

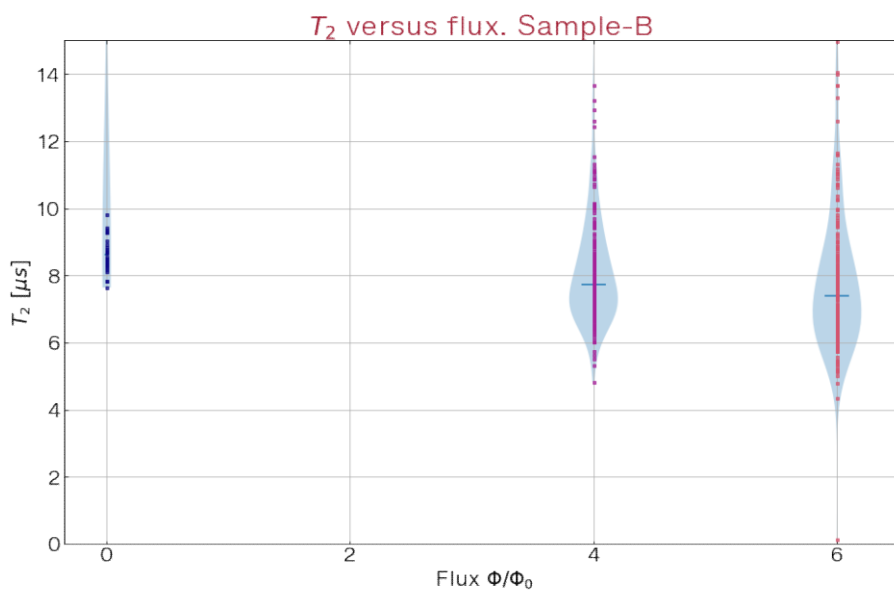


Figure 6.21. Here is T2 vs flux

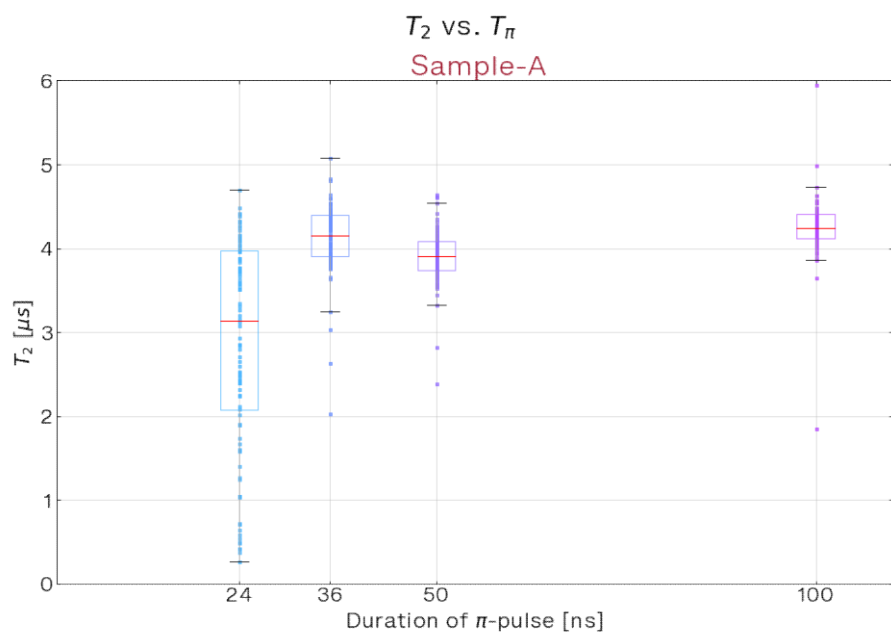


Figure 6.22. T2 statistics

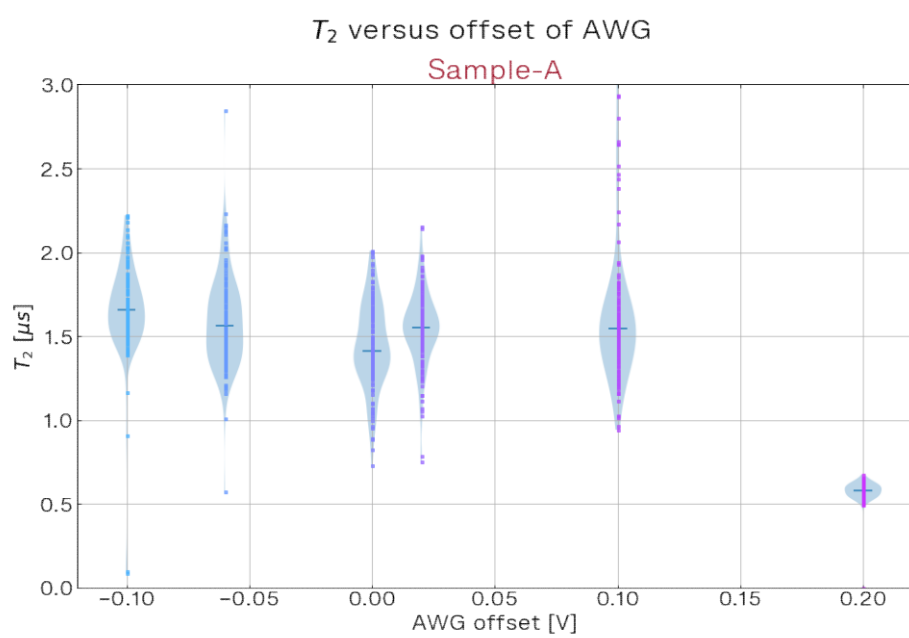


Figure 6.23.  $T_2$  statistics

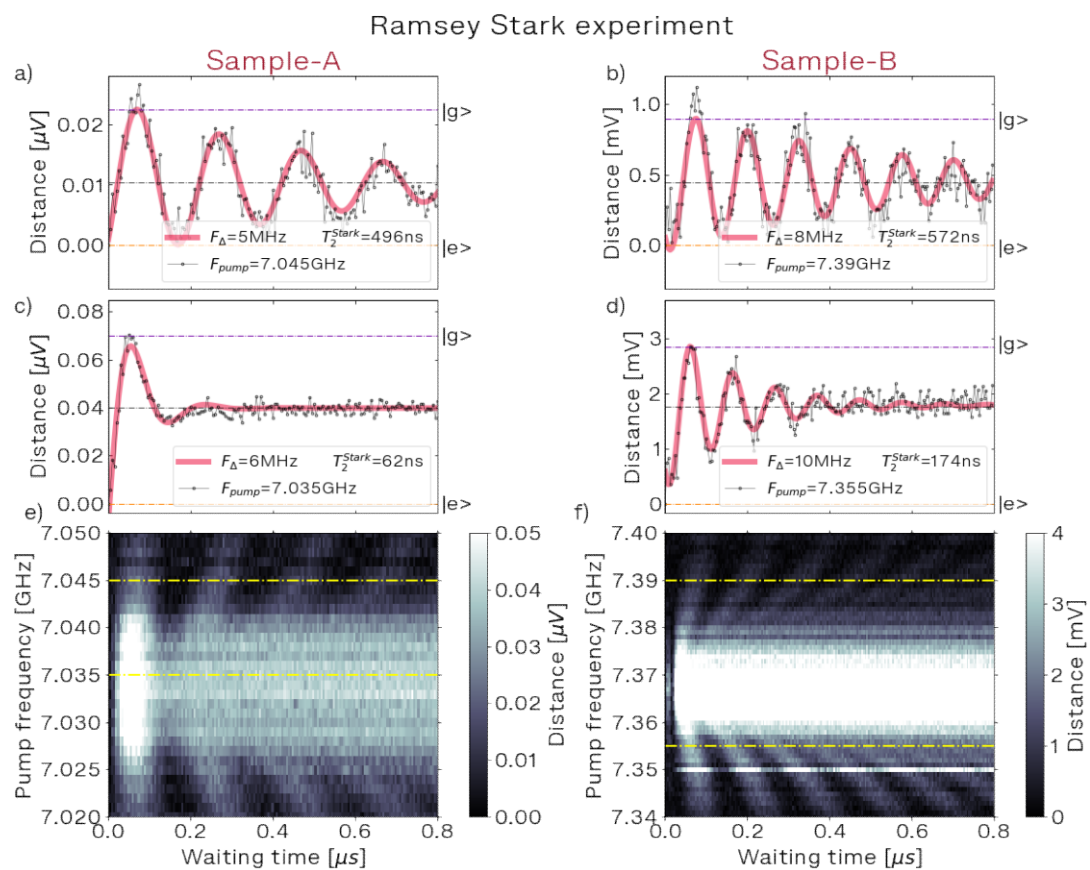


Figure 6.24. Ramsey Stark fringes AB

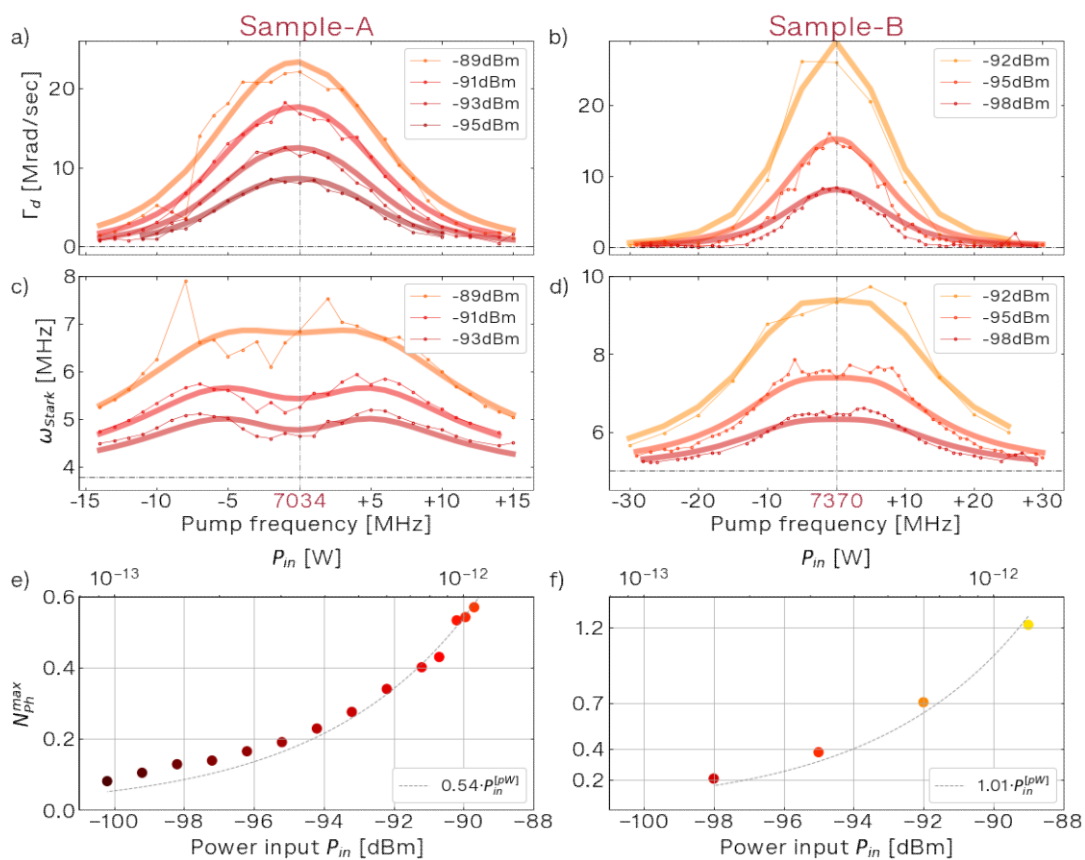


Figure 6.25. Calibration N of photons

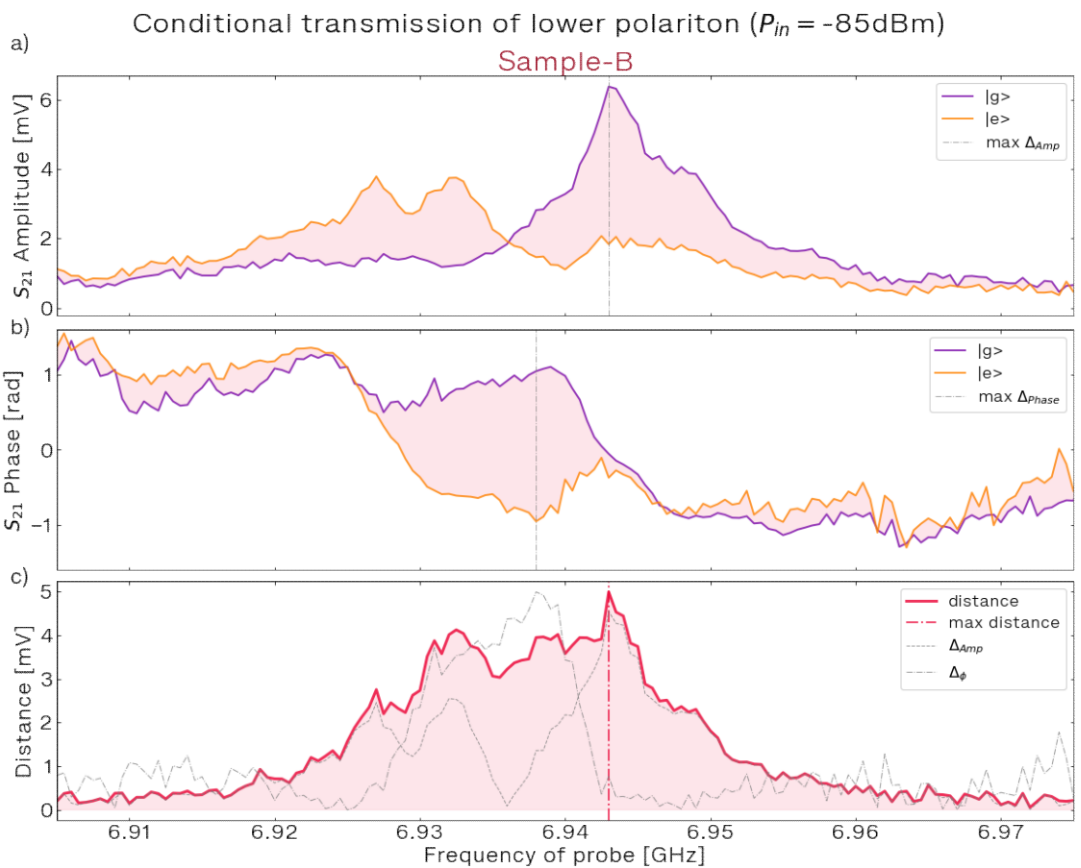


Figure 6.26. Conditional transmission example

Conditional transmission of lower polariton vs probe frequency and power  $P_{in}$   
Sample-B

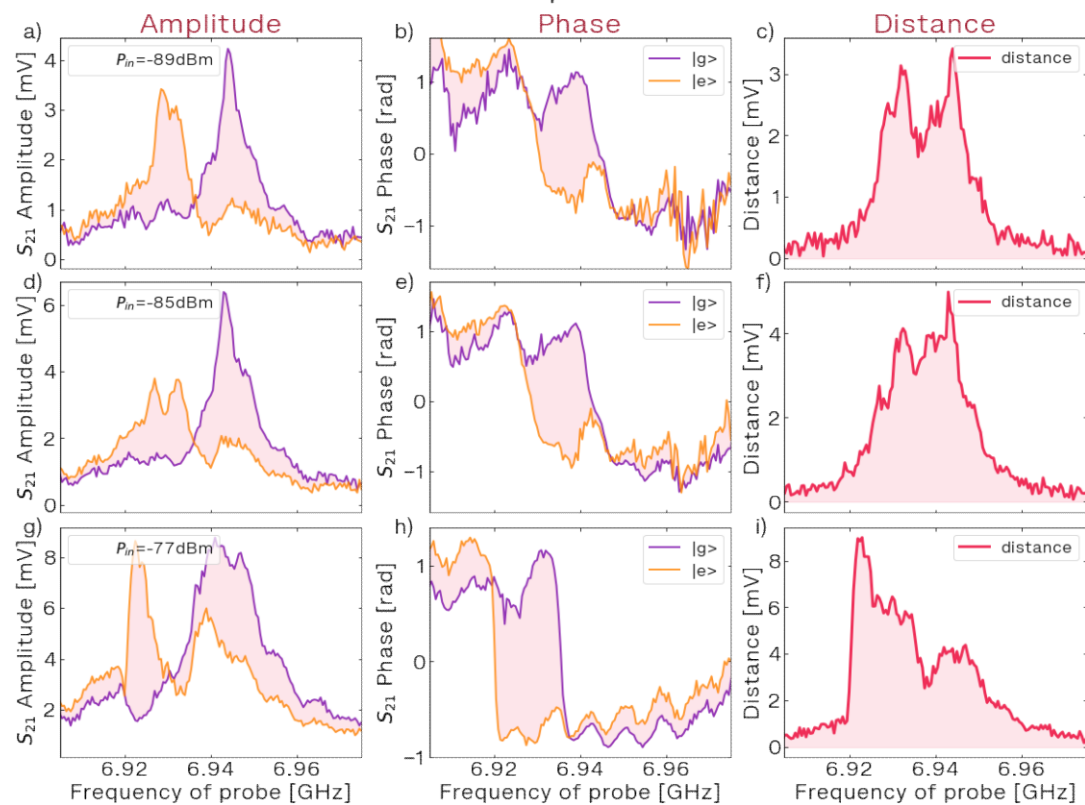


Figure 6.27. Conditional transmission example vs parameters

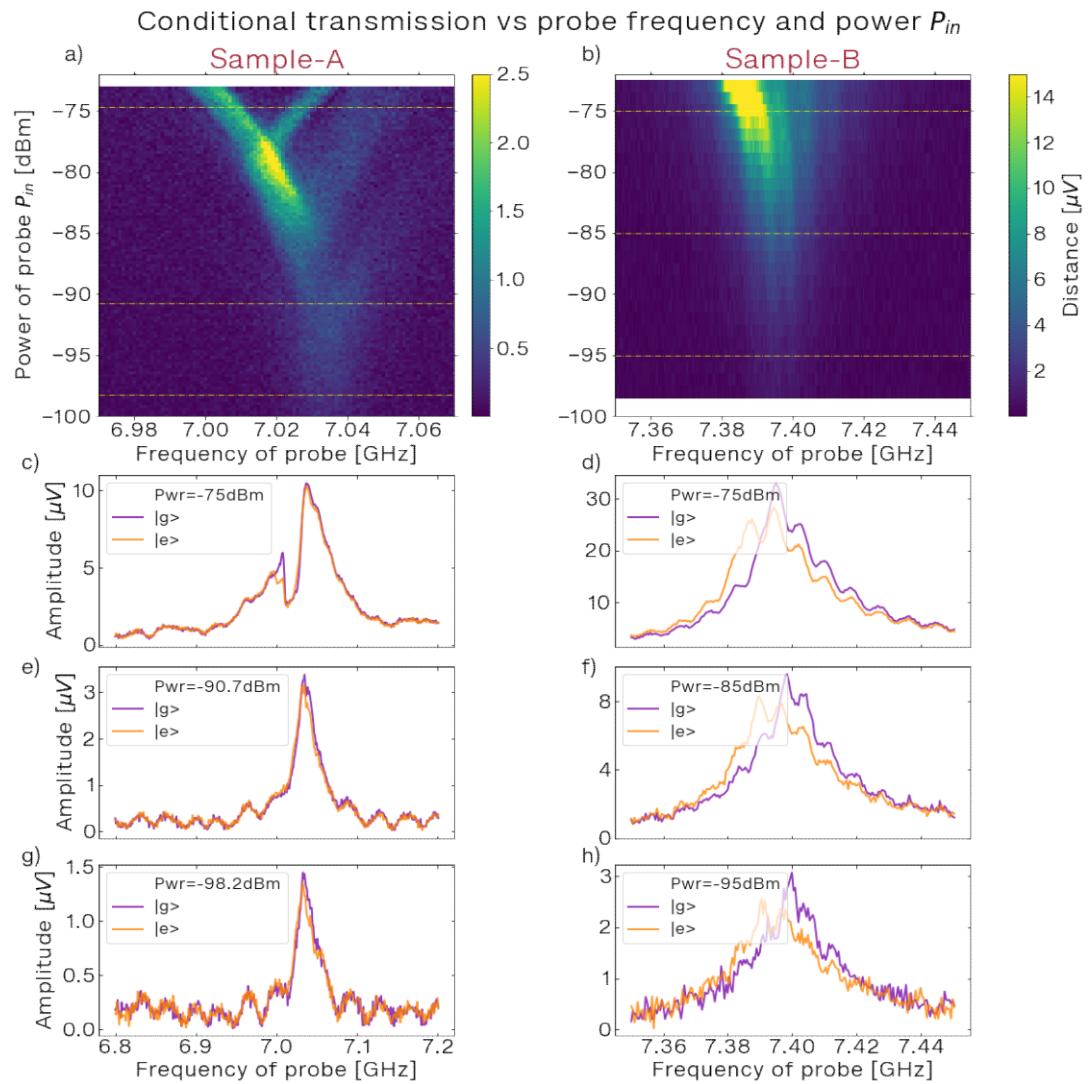


Figure 6.28. Conditional transmission example vs Rudat

Cross-Kerr strengths between qubit and lower ( $\chi_l$ ) and upper ( $\chi_u$ ) polaritons

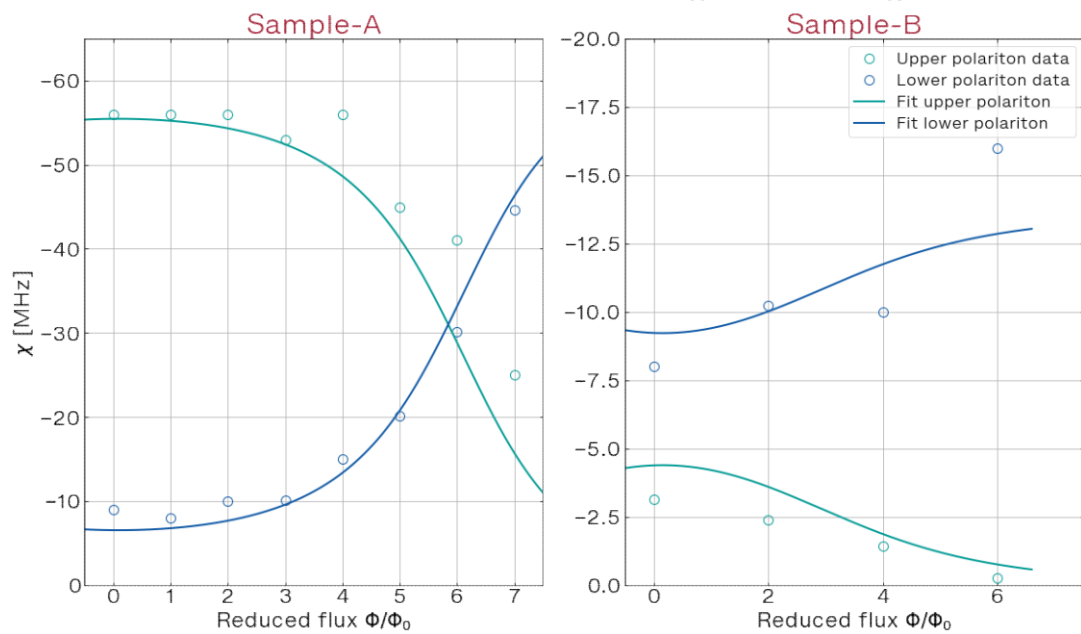


Figure 6.29. Chi vs Flux from cond transmission

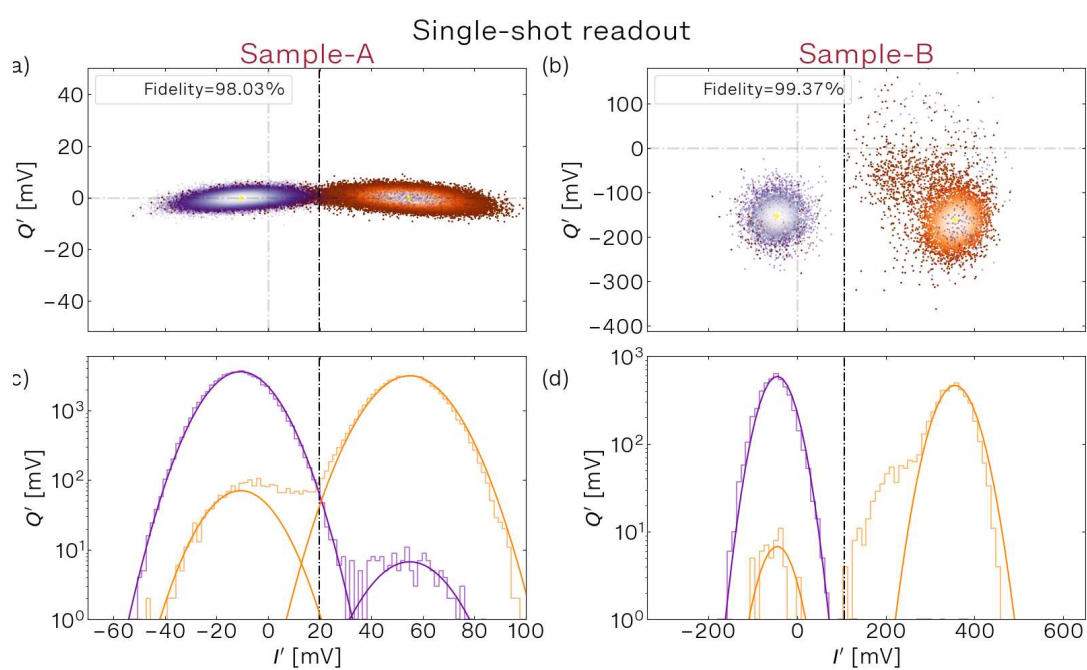


Figure 6.30. Best fidelity A,B

## **6.3. Coherence times of qubit**

**6.3.1. Rabi oscillations -  $T_{pi}$ ,  $T_{Rabi}$**

**6.3.2. Relaxation -  $T_1$**

**6.3.3. Conditional transmission**

**6.3.4. Ramsey oscillations -  $T_2$ , dfreq**

**6.3.5. Spin-echo -  $T2^*$  (if succeed)**

**6.3.6. Results:  $T_1$ ,  $T_2$ , vs Nflux, compare samples**

## **6.4. Qubit state readout via cross-Kerr coupling with polariton**

**6.4.1. Ramsey-stark - Nph, k, chi**

**6.4.2. Conditional transmission (vs Rudat) - chi**

**6.4.3. Single-shot readout - $\zeta$  fidelity**

SSR vs Time, FreqR, Nph

**6.4.4. Quantum trajectories - QNDness, transition rates**

(from Timothee work):description of processing

Gamma-retes vs Nph

**6.4.5. QNDness by seria of single shot readouts**

## **6.5. Chapter key points**

In this chapter we presented results of microwave measurements of three samples. As the spectroscopic measurements of the "A" and "B" samples showed, we achieved the goal set in the [3](#) chapter. The frequencies of the qubit and ancilla as well as their anharmonicity are in good agreement with the given ones.

During the qubit coherence time studies, a fivefold increase in T1 was found in sample "*B*" compared to sample "*A*". This demonstrates the success of the new design for transmon molecule as a whole. Although it is difficult to judge the portion contribution of each of the changes made. Preliminary data obtained on the "*C*" sample also look promising and demonstrate the validity of the new recipe presented in the Fabrication Chapter 4.

As it was supposed, due to the increase of the lifetime it was possible to expand the limits of the possible for reading the state of the given transmon molecule. For the sample "*B*" the results of a single-shot readout with fidelity as high as (!) 99.4% with readout pulse time of 150*ns*. It is also noted that the fidelity values remain high within quite a wide range of variation of duration and power of readout pulse, which was not observed in the case of sample "*A*". Measurements of the sample "*C*" will be carried out in the near future, but drawing attention to the improved coherence characteristics we can expect even better results. The possibility of quantum nondemolition measurement has also been demonstrated to read a qubit state of the transmon molecule.

## **Chapter 7.**

### **Conclusions, Future prospects**

#### **7.1. References, comparison of readout results, Vijays article**

